

# Predicting vortex-induced vibration from driven oscillation results

J.S. Leontini<sup>\*</sup>, B.E. Stewart, M.C. Thompson, K. Hourigan

*Department of Mechanical Engineering, Monash University, Clayton, Australia*

Received 24 January 2005; received in revised form 26 May 2005; accepted 27 May 2005

Available online 2 November 2005

---

## Abstract

Two-dimensional simulations of flow past both an elastically-mounted cylinder and an externally-driven oscillating cylinder were performed at a Reynolds number of  $Re = 200$ . The results were compared to determine if the oscillations of the driven-oscillation model were consistent with the oscillations observed in the elastically-mounted system. It was found that while this is the case, there is considerable sensitivity to input forcing. This sensitivity could explain observed discrepancies between experimental results for the two systems.

© 2005 Elsevier Inc. All rights reserved.

---

## 1. Introduction

Vortex-induced vibration (VIV) of bluff structures can occur whenever a bluff structure is immersed in a fluid stream. If the frequency of this flow-induced vibration is close to a natural frequency of the bluff structure, large-scale oscillations can occur, potentially resulting in the failure of the structure.

In an attempt to study the fundamental aspects of VIV, simplified experimental models are often used. The most common of these is an elastically-mounted cylinder constrained to oscillate transversely to the incoming flow. The behaviour of this system is dependent on a set of non-dimensional parameters including the Reynolds number,  $Re$ , the scaled mechanical system natural frequency,  $f_N^*$ , and the damping ratio,  $\zeta$ . These parameters are defined as follows. The Reynolds number is  $Re = UD/\nu$ , where  $U$  is the freestream velocity,  $D$  is the cylinder diameter, and  $\nu$  is the kinematic viscosity. The natural frequency is  $f_N = \sqrt{k^*/(1 + C_A/m^*)}/2\pi$  where  $k^* = k/m$ ,  $C_A$  is the added-mass coefficient ( $C_A = 1$  for a circular cylinder for *inviscid* flow),  $k$  is the spring constant,  $m$  is the cylinder mass per unit length,  $m^* = m/m_f$ , and  $m_f$  is the mass of displaced fluid. This form of  $f_N$  therefore includes an added-mass effect of the fluid, and is the natural frequency of the submerged cylinder. This can be non-dimensionalised by multiplying by  $D/U$  to give  $f_N^* = f_N D/U$ . Note that while the inviscid added mass is a well-defined constant, the effective added mass can vary significantly in flows associated with vortex-induced vibration [1]. For the cases examined here, the mass ratio is large enough so that the added

---

<sup>\*</sup> Corresponding author.

E-mail address: [justin.leontini@eng.monash.edu.au](mailto:justin.leontini@eng.monash.edu.au) (J.S. Leontini).

mass correction to the natural frequency is relatively small. Finally, the damping ratio is defined as  $\zeta = c / (4\pi m f_N)$  where  $c$  is the mechanical damping constant.

Many studies have been made of this system, including the early work of [2], and the recent studies of [3,4]. An extensive recent review is given in [1]. While simplified, this model is still subject to the complexity of coupled fluid–structure interaction.

It is possible to write down an equation of motion for the coupled fluid–structure system with the body force applied by the fluid as a right-hand side forcing term, and the left-hand side including the spring force and damping force of the mechanical system. Thus the system can effectively be decoupled, although, of course, the fluid forcing is a function of the mechanical setup of the system. From this point of view, given the form of the fluid-forcing signal, it should be possible to accurately predict the motion that the elastically-mounted cylinder would undergo. In particular, if the forcing is sinusoidal, by running a series of models with different forcing amplitudes it should be possible to predict the response of the elastically-mounted case. This can be done by monitoring the energy transfer from the fluid to the cylinder over a cycle for each model. If the energy transfer for a particular model matches the energy loss due to damping, then the predicted amplitude should correspond to that observed in the elastically-mounted case.

The forced system is dependent upon  $Re$ , the normalised amplitude  $A^* = y_{\max}/D$ , where  $y_{\max}$  is the transverse oscillation amplitude, and the normalised frequency of oscillation,  $f^* = fD/U$ , where  $f$  is the frequency of oscillation. The transverse driven oscillating cylinder has been studied by many authors, including [5–7].

The agreement between the predicted amplitude responses from driven-oscillation experiments, and observed responses from VIV experiments, is not always good, even when the vorticity structure of both wakes appear to resemble each other quite closely. In particular, the predicted energy transfer over a cycle appears to be in contradiction. The *energy transfer* is quantified as the work done on a unit length of the cylinder by the fluid over one cycle of oscillation. This is given by

$$E = \int_T F_L v dt, \tag{1}$$

where  $E$  is the work done over the period  $T$ ,  $F_L$  is the lift force per unit length,  $v$  is the transverse velocity and  $t$  is the time. This equation can be normalised to the form

$$C_E = \int_{T^*} C_L v^* d\tau \tag{2}$$

where  $C_E$  is the energy transfer coefficient,  $T^* = TU/D$  is the normalised period,  $C_L = F_L/(1/2\rho U^2 D)$  is the lift coefficient, and  $\rho$  is the fluid density,  $v^* = v/U$  is the normalised transverse velocity, and  $\tau = tU/D$  is normalised time.

During experiments, the sign of  $C_E$  is inferred from the sign of the phase angle between the lift force on the cylinder, and the cylinder displacement. The reasoning for this inference can be found in [8].

Given this reasoning, some attempts have been made at directly predicting VIV from driven oscillation results. The study of [9] had only limited success, and prescribed a limiting maximum amplitude during VIV that has since been exceeded [10]. A later study [11] only found agreement between predictions and experiments over a small range of oscillation frequencies. The more recent direct comparison of [12] showed these discrepancies quite clearly. In a recent review this discrepancy led [13] to ponder whether it was at all possible to model VIV with pure-tone driven oscillation.

The results presented in this paper were obtained at a Reynolds number  $Re = 200$ , using two-dimensional simulations. The results indicate that at this value of  $Re$  driven-oscillation predictions can be consistent with the energy transfer characteristics of VIV, if the values of the input parameters,  $A^*$  and  $f^*$  are matched closely to the values obtained during VIV. It is shown that changes in either the value of  $A^*$  or  $f^*$  of the order of 1% can result in a change in the value of  $C_E$  of 25% during driven oscillation. While these results are two-dimensional and laminar, it is hypothesised that this level of sensitivity could explain the discrepancy between the two systems during higher  $Re$  experiments.

## 2. Computational method

### 2.1. Mathematical formulation

The incompressible Navier–Stokes equations are solved in an accelerated frame of reference attached to the cylinder in both the VIV and driven-oscillation simulations. To allow this, an extra (non-inertial) forcing term is introduced into the momentum equation rendering the system to be solved as

$$\frac{\partial \mathbf{v}}{\partial \tau} = \nabla P + \frac{1}{Re} (\nabla^2 \mathbf{v}) - (\mathbf{v} \cdot \nabla) \mathbf{v} + \frac{d\mathbf{u}_F}{d\tau} \mathbf{j} \quad (3)$$

and

$$\nabla \cdot \mathbf{v} = 0, \quad (4)$$

where  $\mathbf{v}$  is the non-dimensional velocity,  $\tau$  is non-dimensional time,  $P$  is the kinematic pressure and  $d\mathbf{u}_F/d\tau \mathbf{j}$  is the introduced forcing term, which is just the acceleration of the reference frame.

### 2.2. Time advancement

A high-order three-step time-splitting scheme was employed in the solution of the velocity and pressure field for both the VIV and driven-oscillation flows. The three steps account for the advection, pressure and diffusion terms of the Navier–Stokes equation. The pressure and diffusion terms were treated the same way for both problems. The pressure field was evaluated by forming a Poisson equation by taking the divergence of the equation for the pressure, and enforcing continuity at the end of the substep. The diffusion term was evaluated with the theta form of the Crank–Nicholson scheme. This results in a Helmholtz equation. Both the Poisson equation for the pressure and the Helmholtz equations for the viscous terms, lead to linear matrix problems, once the equations are discretised in space. The matrices are inverted at the start of the timestepping procedure; subsequently, the effects of continuity (pressure) and viscous diffusion at each timestep only involve matrix multiplies.

Because the convection term is nonlinear, it is generally treated with an explicit (third-order) Adams–Bashforth method. For the VIV case, there is strong coupling between the fluid and the structural response. The explicit approach becomes unstable and the overall timestepping has to be treated semi-implicitly. This is done by iterating through the three substeps and structural update until the velocity and pressure fields, and the cylinder motion converge. Note that except for the first iteration, the advection term is treated by a semi-implicit Adams–Moulton method, which improves the stability. Typically, it takes two or three outer iterations to establish convergence, however, the timestep can generally be chosen to up to an order of magnitude greater than the Courant timestep, which controls the non-iterative approach used for the forced oscillation simulations.

For the VIV simulations, the motion of the cylinder was solved as part of the solution procedure. The following equation governs the motion:

$$m\ddot{y} + cy + ky = F_L. \quad (5)$$

For the driven-oscillation problem, the cylinder position at any time was prescribed by the driving function,

$$y = y_{\max} \cos(2\pi f\tau), \quad (6)$$

where  $y_{\max}$  and  $f$  were prescribed through  $A^*$  and  $f^*$ . This allowed the additional forcing term in the Navier–Stokes equations to be expressed explicitly. Further details of the time-splitting method can be found in [14,15].

### 2.3. Spatial discretisation

A spectral-element technique was employed for all the simulations performed. The spatial domain was discretised into 508 elements, with the majority concentrated in the wake and boundary-layer regions. Some care was taken to construct a near-optimal mesh, and domain size and resolution studies were conducted to validate the predictions. This macro-element mesh is shown in Fig. 1. Within each element, the mesh geometry,

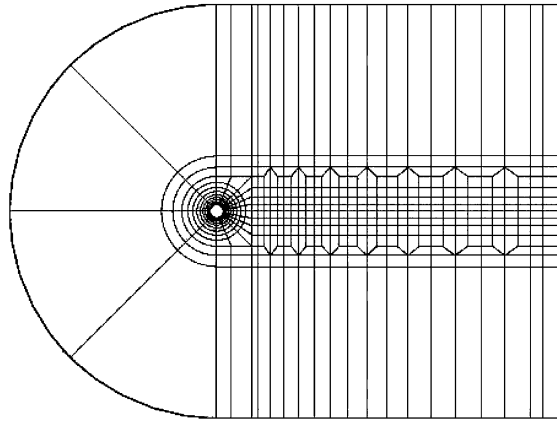


Fig. 1. The mesh used for both the VIV and driven-oscillation simulations.

as well as the velocity and pressure fields, were represented by eighth-order tensor-product polynomials, associated with Gauss–Lobatto–Legendre quadrature points. Details of the approach and implementation have been provided elsewhere, e.g., [15,16].

Boundary conditions were set to  $u = U$  and  $v = v_{\text{cyl}}$  at the inlet, top and bottom boundaries, where  $u$  and  $v$  are the  $x$  and  $y$  velocity components, respectively, and  $v_{\text{cyl}}$  is the cylinder velocity. At the cylinder wall, a no-slip condition was imposed. Higher-order boundary conditions [14] are used for the pressure gradient at no-slip boundaries and at the far-field boundaries. At the outlet, the pressure is fixed and the normal velocity gradient is set to zero.

### 3. Results

#### 3.1. Vortex-induced vibration

To allow a comparison between vortex-induced vibration (VIV) and driven-oscillation predictions, a set of VIV results were first obtained. For all of these simulations, a mass ratio of  $m^* = 10$  was used, where  $m^*$  is the ratio between the mass of the cylinder structure and the mass of displaced fluid. A damping coefficient was used that yielded a damping ratio of  $\zeta = 0.01$ , resulting in a combined mass-damping parameter of  $m^*\zeta = 0.1$ .

The natural frequency of the mechanical system,  $f_N$ , was varied by altering the value of the spring constant,  $k$ . Three distinct regions of amplitude response were observed, with the highest magnitude response occurring at values of  $f_N$  close or equal to the shedding frequency, or Strouhal frequency, of a stationary cylinder,  $f_{St}$ . At these values of  $f_N$ , the shedding frequency of the wake and the oscillation frequency of the cylinder were observed to synchronise with approximately the natural frequency of the structure,  $f \approx f_N$ . This response regime was labelled the synchronisation region. Outside this region, shedding and the cylinder oscillation was at approximately the same frequency as the shedding from a fixed cylinder,  $f \approx f_{St}$ .

This synchronisation region can be clearly identified in Fig. 2a and b. Fig. 2a shows  $A^*$  plotted against the normalised natural frequency  $f_N^*$ . This plot clearly shows the sudden jump to larger amplitudes corresponding to the onset of synchronisation, and the sudden decrease in amplitude of oscillation with the loss of synchronisation. Fig. 2b shows the ratio of response frequency  $f$  to the natural frequency  $f_N$ , plotted against the normalised response frequency  $f^*$ . This plot shows the sudden synchronisation of the wake to the natural frequency, as the natural frequency approaches the wake-shedding frequency of the stationary cylinder,  $f_{St}$ .

#### 3.2. Synchronisation during driven oscillation

Presented in Fig. 3a are the synchronisation boundaries for the driven cylinder case, in the  $A^*$  versus  $f^*$  plane. Synchronisation during driven oscillation is caused by the motion of the cylinder overriding the

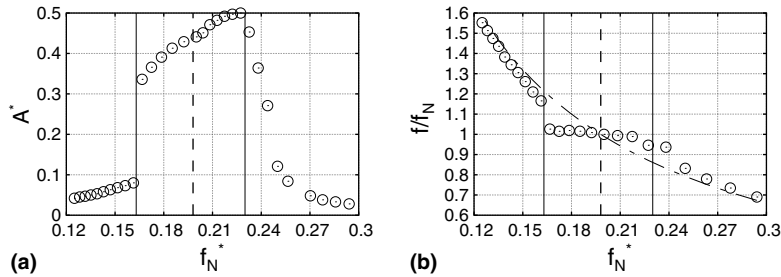


Fig. 2. (a)  $A^*$  versus normalised natural frequency. The largest amplitudes occur between  $f_N^* = 0.16$  and  $f_N^* = 0.22$ , bracketing the shedding frequency from a stationary cylinder,  $f_{St}$  (---). (b) The ratio of response frequency  $f$  to natural frequency  $f_N$ , versus normalised natural frequency  $f_N^*$ . Over the frequency range  $f_N^* = 0.16$  and  $f_N^* = 0.22$ , the wake synchronises with the natural frequency, resulting in the larger oscillation amplitudes. The dash-dot line (— · —) is  $f_{St}/f_N^*$ , showing that outside the synchronisation region, the vortices shed at approximately the fixed cylinder frequency,  $f_{St}$ .

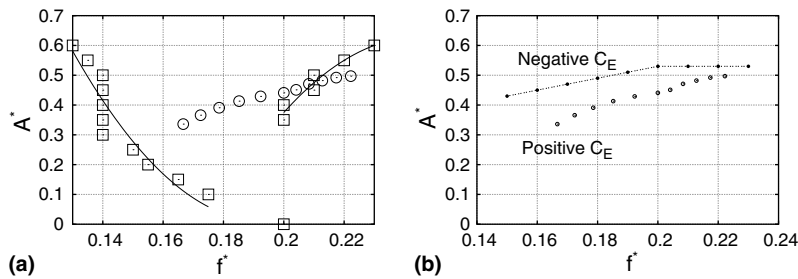


Fig. 3. (a) Synchronisation boundaries for the driven oscillation case. (□) represents data points used for synchronisation boundary. (—) represents line of best fit for synchronisation boundary. (○) represents VIV synchronised cases. Almost all the VIV cases fall within the synchronisation limits of the driven oscillation, indicating the driven oscillation case can be used as an indicator of synchronisation in VIV. (b) Energy transfer directions for the driven oscillating cylinder. (●) represents  $C_E = 0$ . (○) represents VIV amplitudes of oscillation. It is shown that all the VIV cases occur in the positive  $C_E$  region, but close to the upper boundary.

shedding frequency from a stationary cylinder,  $f_{St}$ . It is therefore the cylinder oscillation frequency that controls the oscillation of the wake. The fact that the VIV results mainly fall inside this boundary implies that the cylinder oscillation controls the wake oscillation during synchronised VIV.

While the lower frequency synchronisation boundary presented in Fig. 3a is well defined, the upper boundary is not and requires further work to clearly define. This boundary is difficult to define due to the high sensitivity of the system to input frequency. For a given amplitude, varying the normalised oscillation frequency by as little as 1% could change the magnitude of the lift force on the cylinder by as much as 25%.

In this same region of parameter space, it is also observed that the VIV results fall outside the driven oscillation synchronisation boundary. This is not so surprising, as the VIV oscillation is moving further from a pure sinusoid in this region, acquiring a significant variation in amplitude over time that is not purely periodic. All the VIV results that fall inside the synchronisation boundaries of the driven oscillation are very close to purely sinusoidal, suggesting that the points outside the boundary are not completely synchronised, but undergoing a transition, with intermittent periods of synchronisation interspersed with periods of unsynchronised vortex shedding.

### 3.3. Energy transfer during driven oscillation

For driven oscillation to be a useful model of VIV, it needs to exhibit similar energy transfer characteristics to the VIV case. During steady-state, synchronised VIV, the overall energy transfer to the mechanical system must be zero. Alternatively, the work done on the cylinder by the fluid will be equal to the work dissipated by mechanical damping. Hence,  $C_E$  during VIV retains the same definition as during driven oscillation. For

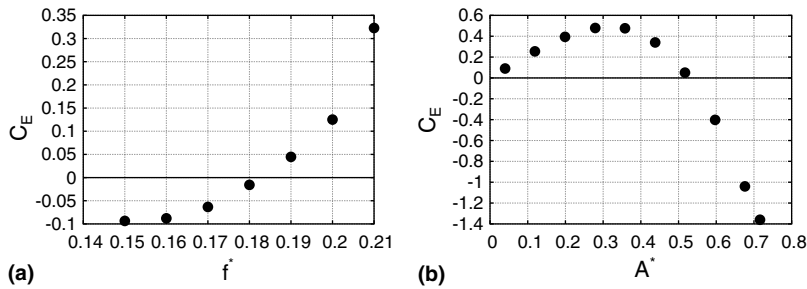


Fig. 4. (a)  $C_E$  against  $f^*$ ,  $A^* = 0.5$ . Once positive,  $C_E$  quickly increases with increasing  $f^*$ . (b)  $C_E$  against  $A^*$ ,  $f^* = 0.2$ . As  $A^*$  approaches the value where there is a change from positive to negative  $C_E$ , it is shown that  $C_E$  varies steeply.

driven oscillation to model VIV, it must return a positive value of  $C_E$  in regions of the  $A^*, f^*$  plane where VIV occurs. For this study,  $C_E$  was only calculated during synchronisation, hence the value of  $C_E$  was the same for any period of oscillation.

Fig. 3b shows a line of  $C_E = 0$ , effectively dividing the  $A^*, f^*$  plane into  $C_E > 0$  and  $C_E < 0$  zones. It shows an upper limit on  $A^*$  for  $C_E > 0$ , indicating a limit on the amplitude possible during VIV, if the driven oscillation is modelling VIV accurately.

Also plotted are the amplitudes of VIV cases, and all of these fall in the  $C_E > 0$  region. This result is encouraging, and indicates that at the  $Re$  tested, the driven oscillation using a pure-tone oscillation is capturing the energy transfer characteristics of VIV. It also shows that the VIV cases occur close to the transition from positive to negative  $C_E$ . The small positive difference can be attributed to the energy required by the system to account for energy lost through damping.

The proximity of the VIV cases to the boundary between positive and negative  $C_E$  again highlights the importance of matching the input frequency closely, as high gradients of  $C_E$  during driven oscillation are observed in this area of the parameter space.

This sensitivity is shown in Fig. 4. Fig. 4a shows the change in  $C_E$  with increasing frequency for a fixed amplitude. It is shown that as soon as  $C_E$  becomes positive, it rapidly increases with increasing frequency  $f^*$ .

Fig. 4b shows the change in  $C_E$  with increasing amplitude for a fixed frequency in the synchronisation range. Here,  $C_E$  displays a sensitive dependence on the value of  $A^*$ , especially as  $A^*$  approaches  $A^* > 0.35$ . This range of  $A^*$  is that experienced during synchronised VIV. The high sensitivity of the  $C_E$  value of the driven oscillation system on its input parameters highlights the difficulty in using driven oscillation results to predict or model VIV. Changes in the input parameters ( $A^*$  and  $f^*$ ) of the order of 1% can result in changes of  $C_E$  of up to 25%, or in it reversing sign.

#### 4. Conclusions

Experimental work has been unable to capture all of the characteristics of vortex-induced vibration, especially the energy transfer characteristics. However, this numerical study has made good progress, showing that for the parameter regime considered here at least, VIV occurs where it is predicted by driven oscillation, and the behaviour VIV causes is well predicted by driven oscillation simulations.

This numerical study has shown that the driven oscillating system is highly sensitive to the amplitude of oscillation  $A^*$ , and the oscillation frequency  $f^*$ , especially in the region of parameter space where VIV occurs. Changes of the order of 1% in either can change the magnitude of the energy transfer coefficient,  $C_E$ , by the order of 25%. In some critical instances, this can also result in the sign of  $C_E$  reversing.

While the Reynolds number,  $Re$ , is low compared to experiments, the discovery of this high sensitivity could help to provide an explanation as to why driven oscillation experiments predict VIV should not occur when it actually occurs at its largest amplitudes. It remains to be seen whether three-dimensional simulations at higher Reynolds number can improve the predictions made.

## Acknowledgements

Primary support for this research program was provided by the Monash University Engineering Research Committee. Mr. Leontini also acknowledges support from the Department of Mechanical Engineering, Monash University, through a Departmental Postgraduate Scholarship.

## References

- [1] T. Sarpkaya, A critical review of the intrinsic nature of vortex-induced vibrations, *J. Fluids Struct.* 19 (2004) 389–447.
- [2] C.C. Feng, The measurement of vortex-induced effects in flow past a stationary and oscillating circular and d-section cylinders, Master's thesis, University of British Columbia, 1968.
- [3] A. Khalak, C.H.K. Williamson, Motions, forces and mode transitions in vortex-induced vibrations at low mass-damping, *J. Fluids Struct.* 13 (1999) 813–851.
- [4] R. Govardhan, C.H.K. Williamson, Modes of vortex formation and frequency response of a freely vibrating cylinder, *J. Fluid Mech.* 420 (2000) 85–130.
- [5] R.E.D. Bishop, A.Y. Hassan, The lift and drag forces on a circular cylinder oscillating in a flowing fluid, *Proc. Roy. Soc. London, Ser. A* 277 (1368) (1964) 51–75.
- [6] C.H.K. Williamson, A. Roshko, Vortex formation in the wake of an oscillating cylinder, *J. Fluids Struct.* 2 (1988) 355–381.
- [7] J. Carberry, J. Sheridan, D. Rockwell, Forces and wake modes of an oscillating cylinder, *J. Fluids Struct.* 15 (2001) 523–532.
- [8] J. Carberry, Wake states of a submerged oscillating cylinder and of a cylinder beneath a free surface, Ph.D. thesis, Monash University, 2001.
- [9] T. Sarpkaya, Fluid forces on oscillating cylinders, *J. Waterways, Port, Coastal Ocean Div. ASCE* 104 (1978) 275–290.
- [10] A. Khalak, C.H.K. Williamson, Dynamics of a hydroelastic cylinder with very low mass and damping, *J. Fluids Struct.* 10 (1996) 455–472.
- [11] T. Staubli, Calculation of the vibration of an elastically mounted cylinder using experimental data from forced oscillation, *J. Fluids Eng.* 105 (1983) 225–229.
- [12] J. Carberry, J. Sheridan, D. Rockwell, A comparison of forced and free oscillating cylinders, in: *Proceedings of the 14th Australasian Fluid Mechanics Conference*, 2001, pp. 701–704.
- [13] C.H.K. Williamson, R. Govardhan, Vortex-induced vibrations, *Annu. Rev. Fluid Mech.* 36 (2004) 413–455.
- [14] G.E. Karniadakis, M. Israeli, S.A. Orszag, High-order splitting methods of the incompressible Navier–Stokes equations, *J. Comput. Phys.* 97 (1991) 414–443.
- [15] M.C. Thompson, K. Hourigan, J. Sheridan, Three-dimensional instabilities in the wake of a circular cylinder, *Exp. Thermal Fluid Sci.* 12 (1996) 190–196.
- [16] K. Ryan, M.C. Thompson, K. Hourigan, Three-dimensional transition in the wake of bluff elongated cylinders, *J. Fluid Mech.* 538 (2005) 1–29.